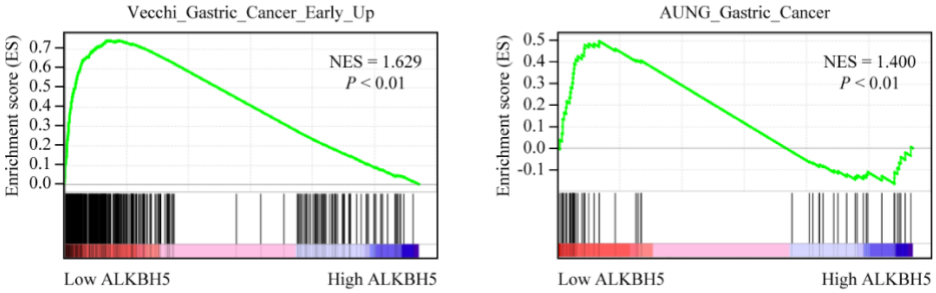

Supplementary Figure S1. Lower ALKBH5 expression was associated with gastric cancer tumorigenesis.

Samples from the GEO dataset (GSE236522) were classified into high- or low-ALKBH5 expression. GSEA was performed to explore the potential biological functions in the high- or low-ALKBH5 groups in STAD tissues.

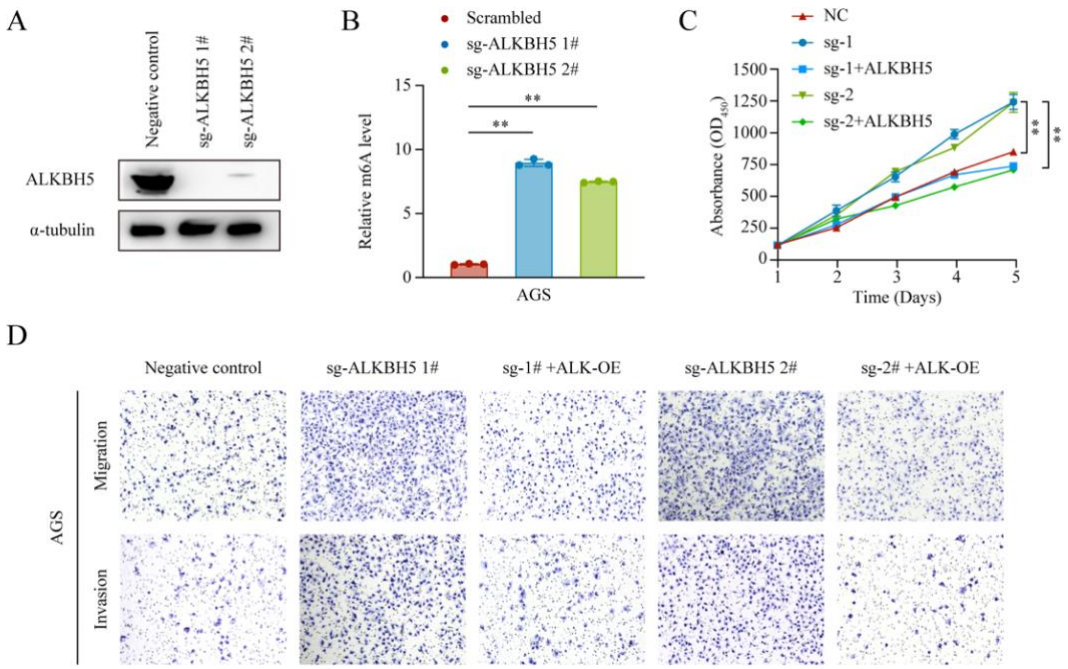

Supplementary Figure S2. Inhibition of ALKBH5 expression promotes the proliferation, migration and invasion of gastric cancer cells.

A–B. Two independent sgRNAs (sg-ALKBH5 #1 and #2) were designed based on the ALKBH5 gene sequence to knockout the ALKBH5 gene in AGS cells. The knockout efficiency was evaluated by Western blot analysis (**A**), and changes in the overall m6A levels of cellular RNA were subsequently assessed (**B**). **C–D.** ALKBH5 was overexpressed in ALKBH5-stably knockout AGS cells to restore its expression levels. CCK-8 assays were used to assess changes in cell proliferation following ALKBH5 restoration (**D**), and Transwell assays were performed to evaluate the effects of ALKBH5 restoration on the migration and invasion abilities of AGS cells (**D**).

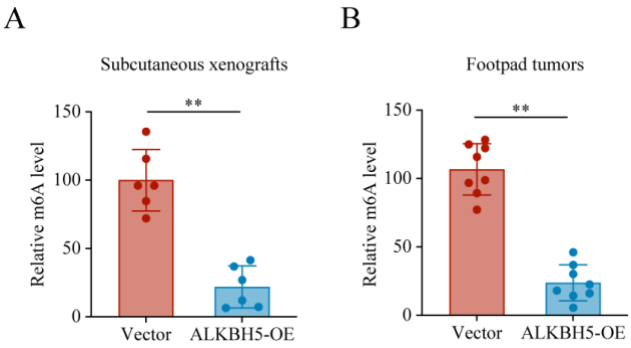

Supplementary Figure S3. Quantification of m6A levels in subcutaneous tumors and footpad tumors in nude mice.

A–B. Subcutaneous xenograft tumor models (**A**) and inguinal lymph node metastasis models (**B**) were established by injecting HGC27 cells with stable ALKBH5 overexpression or control cells into nude mice. The tumors were harvested for m6A quantification. $^{**}P < 0.01$.

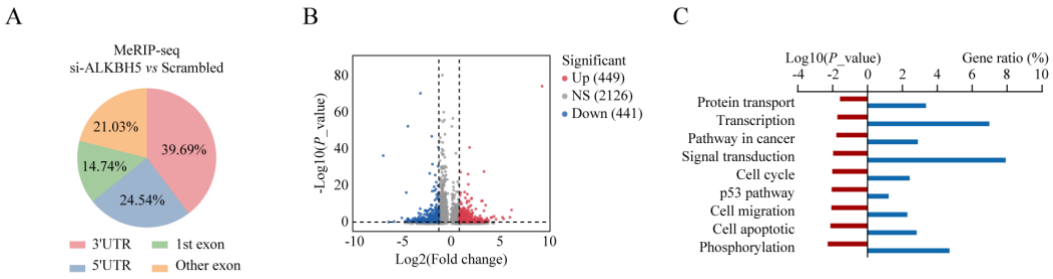

Supplementary Figure S4. MeRIP-seq in AGS cells with or without ALKBH5 silenced.

A-C. AGS cells with or without ALKBH5 knockdown were subjected to MeRIP-seq analysis. (**A**) Pie chart depicting the distribution of differential m6A modifications following ALKBH5 knockdown. (**B**) Volcano plot showing the differentially modified genes after ALKBH5 knockdown, defined as those with *P*-value < 0.05 and |Log2(Fold change) | ≥ 1. (**C**) GO and KEGG pathways enrichment analysis of differentially m6A-modified genes identified by MeRIP-seq.

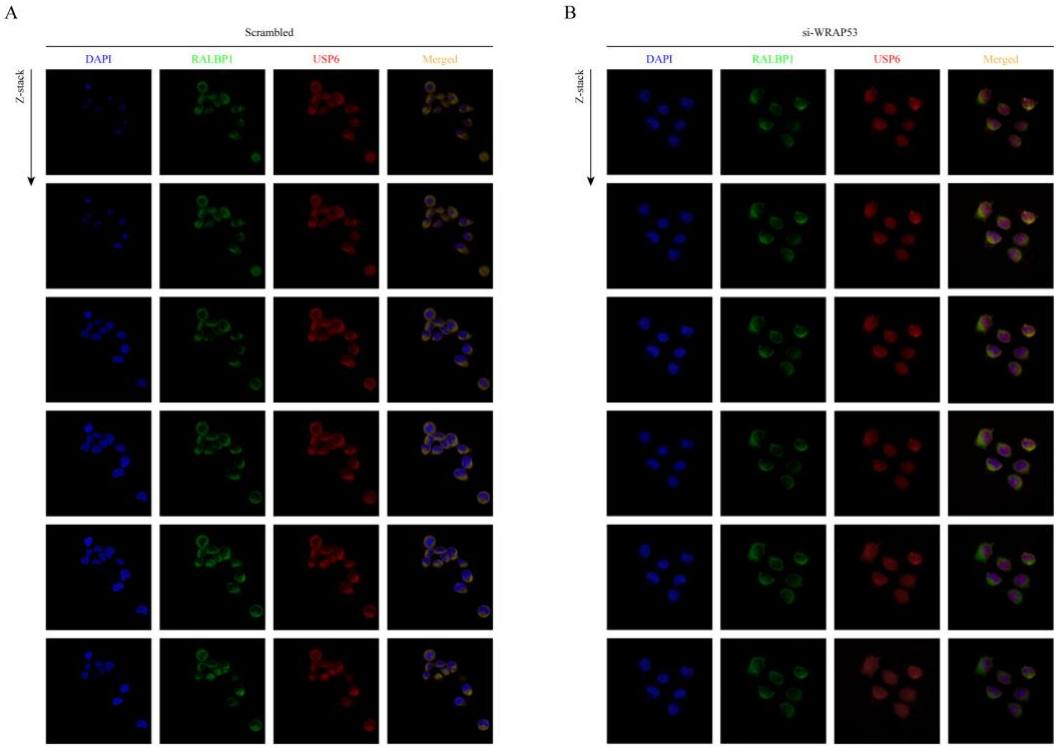

Supplementary Figure S5. Z-Stack of HGC27 cells reflecting the co-localization of RALBP1 and USP6.

A–B. Z-stack imaging was performed using a laser confocal microscope (Zeiss LSM-880 Fast AiryScan, Germany). Images were captured across multiple planes, from the upper to lower layers of the cells. RALBP1 is shown in green (fluorescent secondary antibodies), USP6 is also shown in red (fluorescent secondary antibodies), and nuclei are stained blue with DAPI. Each successive image was captured at a depth 1 μm deeper than the previous one, as indicated by the arrow. HGC27 cells transfected with si-scrambled (**A**) or si-WRAP53 (**B**).

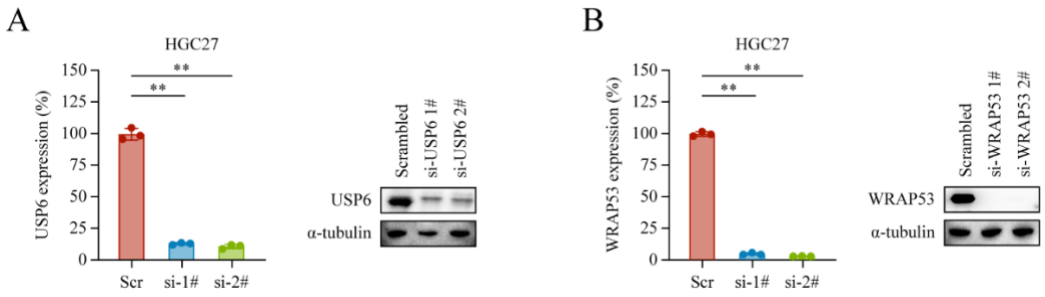

Supplementary Figure S6. Verification of siRNA USP6 and WRAP53 knockdown efficiency.

A–B. Two independent siRNAs targeting USP6 (**A**) and WRAP53 (**B**) were transiently transfected to HGC27 cell. Then, the silencing efficiency of each siRNA was determined by qPCR (left panel) and Western blotting (right panel) analysis. $^{**}P < 0.01$